# Exchange Coupling Interaction in $L1_0$-FePd/α-Fe Nanocomposite Magnets with Large Maximum Energy Products

**Noritsugu Sakuma,[†] Tsubasa Ohshima,[‡] Tetsuya Shoji,[†] Yoshihito Suzuki,[‡] Ryota Sato,[‡] Ayako Wachi,[‡] Akira Kato,[†] Yoichiro Kawai,[†] Akira Manabe,[†] and Toshiharu Teranishi[‡,*]**

[†]Advanced Material Engineering Division, Toyota Motor Corporation, 1200 Mishuku, Susuno, Shizuoka 410-1193, Japan, and [‡]Graduate School of Pure and Applied Sciences, University of Tsukuba, 1-1-1 Tennodai, Tsukuba, Ibaraki 305-8571, Japan

**ABSTRACT** Nanocomposite magnets (NCMs) consisting of hard and soft magnetic phases are expected to be instrumental in overcoming the current theoretical limit of magnet performance. In this study, structural analyses were performed on $L1_0$-FePd/α-Fe NCMs with various hard/soft volume fractions, which were formed by annealing Pd/$\gamma$-$Fe_2O_3$ heterostructured nanoparticles and pure Pd nanoparticles. The sample with a hard/soft volume ratio of 82/18 formed by annealing at 773 K had the largest maximum energy product ($BH_{max}$ = 10.3 MGOe). In such a sample, the interface between the hard and soft phases was coherent and the phase sizes were optimized, both of which effectively induced exchange coupling. This exchange coupling was directly observed by visualizing the magnetic interaction between the hard and soft phases using a first-order reversal curve diagram, which is a valuable tool to improve the magnetic properties of NCMs.

**KEYWORDS:** nanocomposite magnet · $L1_0$-FePd/α-Fe · heterostructured nanoparticle · maximum energy product · first-order reversal curve diagram

The concept of a nanocomposite magnet (NCM) was reported two decades ago by Coehoorn *et al.*[1] and Skomski *et al.*, whose contribution is known as Skomski's MJ (1 MJ/m$^3$ = 120 MGOe) magnet prediction.[2] This concept is expected to be instrumental in overcoming the current theoretical limit of magnet performance toward advanced permanent magnetic applications. Enhancement of maximum energy product, $(BH)_{max}$, in micronano structured materials can be obtained using ferromagnetic–ferromagnetic or ferromagnetic–antiferromagnetic[3] exchange interactions. Our attention is focused on verification of a principle of ferromagnetic–ferromagnetic exchange spring interactions to utilize NCMs as advanced permanent magnetic materials. Many researchers have attempted to fabricate high performance NCMs and successfully produced some NCMs with enhanced remanence and/or maximum energy product, $(BH)_{max}$.[4] However, most of these works have described only single-loop *M-H* curves and/or the remanence enhancement, and have not discussed the structurally required condition of exchange interaction between the hard and soft phases. When discussing structural characteristics, most of these studies refer to earlier work, which reported that an amorphous phase was necessary for effective exchange coupling and remanence enhancement.[5] In contrast, micromagnetics simulations and theoretical works suggest exchange coupling between hard and soft phases should be rigid, which leads to good squareness and larger $(BH)_{max}$.[2] Rigid exchange coupling should arise from a coherent hard/soft interface, or one that at least has a crystallographic orientation relationship, because the exchange interaction is sensitive to interatomic distance.[6] Obviously there is a discrepancy between the experimental and theoretical results. Therefore, the correlation between the exchange coupling and the structural conditions, such as interface structure, size of soft phase, and volume fraction of hard/soft phases, should be clarified. For this purpose, the FePd system is useful as it has a hard/soft crystalline interface without amorphous phases, as observed in NdFeB melt spinning system[4] or diffuse interface in FePt system.[7–9] Recently, an example of colloidal bimagnetic heterostructured NPs based on coupled soft and hard materials have been reported, namely FePt–iron oxide heterodimers, which showed the signature of magnetic exchange-spring interactions.[10] The advantage of the FePd system lies in its phase diagram (Supporting Information, Figure S1), which illustrates that this system has a composition range, in which $L1_0$-FePd and α-Fe phases can exist simultaneously as a thermodynamically stable state. This indicates that this system is suitable for obtaining a stable hard/soft nanocomposite structure.

Here we report average structural information from X-ray diffraction (XRD) and

* Address correspondence to teranisi@chem.tsukuba.ac.jp.

Received for review December 1, 2010 and accepted March 22, 2011.

**Published online March 22, 2011**
10.1021/nn103286r

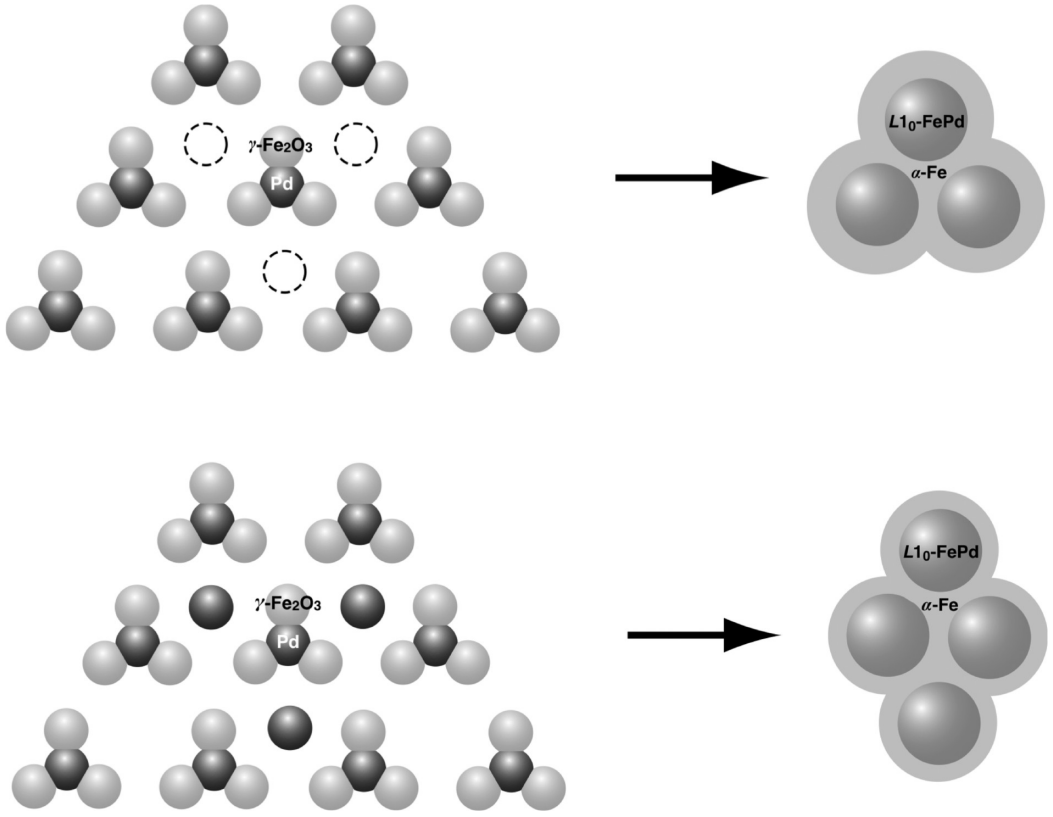


**Figure 1. Schematic illustration of the formation of FePd/Fe NCMs with different FePd/Fe volume ratios from the mixture of Pd/$\gamma$-$Fe_2O_3$ heterostructured NPs and pure Pd NPs.**

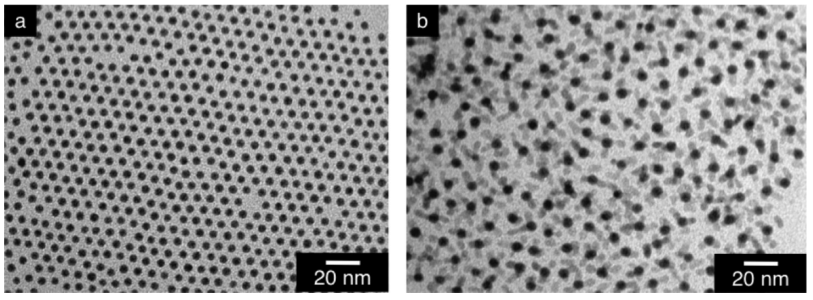


**Figure 2. TEM images of (a) 4.9 $\pm$ 0.3 nm Pd NPs and (b) Pd/$\gamma$-$Fe_2O_3$ heterostructured NPs with a Fe/Pd molar ratio of 80/20.**

microstructural images from transmission electron microscopy (TEM) of $L1_0$-FePd/α-Fe NCMs. These NCMs were synthesized *via* interfacial atom diffusion between Pd and α-Fe phases formed by the reductive annealing of $\gamma$-$Fe_2O_3$ phases.[11] The volume fraction of hard ($L1_0$-FePd)/soft (α-Fe) phases was varied from 44/56 to 100/0 by mixing Pd/$\gamma$-$Fe_2O_3$ heterostructured nanoparticles (NPs) with pure Pd NPs (Figure 1). The Pd/$\gamma$-$Fe_2O_3$ heterostructured NPs are advantageous for effective interfacial atom diffusion because the Pd and $\gamma$-$Fe_2O_3$ phases are always neighboring each other.[10−19] In fact, a reductive annealing of a Pd and iron oxide NP mixture gave quite polydisperse NPs having body-centered cubic (bcc) α-Fe and $L1_0$-FePd phases because two kinds of NPs were randomly distributed.[9] A first-order reversal curve (FORC) analysis was used to visualize the exchange interaction to overcome the limitation of the Henkel-plot.[20] By combining the FORC diagram with the microstructural analysis, we discuss both the existence of exchange coupling and the interface structure between the hard and soft phases of the FePd system to obtain the optimized structure of NCMs.

## RESULTS AND DISCUSSION

**Structural Analysis.** TEM images (Figure 2) were obtained of Pd NPs (4.9 $\pm$ 0.3 nm) and Pd/$\gamma$-$Fe_2O_3$ heterostructured NPs with a Fe/Pd molar ratio of 80/20. As observed in earlier studies, the Pd/$\gamma$-$Fe_2O_3$ heterostructured NPs were composed of dark Pd phases with one-to-three bright phases anisotropically grown at every single Pd NP surface, and the size of the

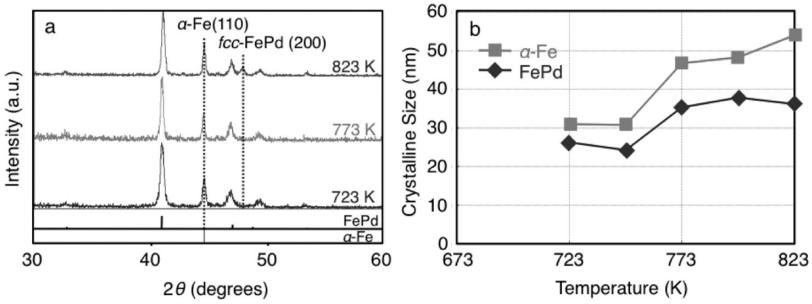


**Figure 3. (a) XRD pattern of FePd/Fe (44/56) NCMs formed by annealing at 723, 773, and 823 K. (b) Crystalline size of FePd (diamond) and α-Fe (square) of FePd/Fe (44/56) NCMs formed by annealing at various temperatures.**

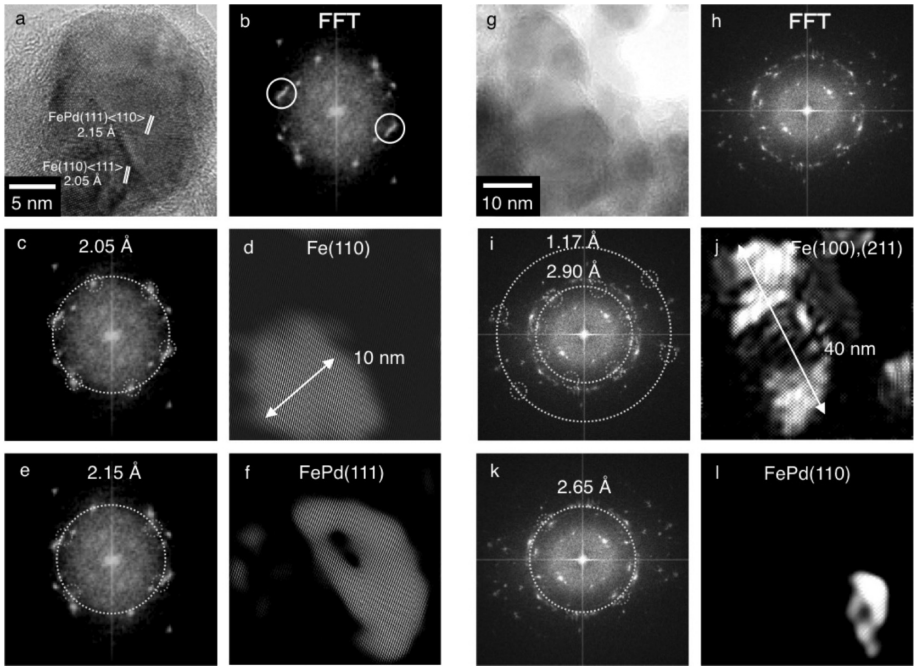


**Figure 4. Structural analysis of FePd/Fe (44/56) NCMs formed by annealing Pd/γ-$Fe_2O_3$ heterostructured NPs at (a−f) 723 K and (g−l) 823 K. (a,g) HRTEM images, (b,h) all FFT spots, (c,e,i,k) distinct FFT spots, and (d,f,j,l) inverse-FFT images corresponding to panels c,e,i,k, respectively. The FFT spots in panels i and k were attributed to Fe(100) and (211) and $L1_0$-FePd(110), respectively, from inverse-FFT analysis (j,l).**

Pd NPs was preserved.[11] These NPs were annealed in $O_3$ to remove surface organic ligands prior to conversion into NCMs. This $O_3$ treatment effectively suppressed both the carbonization of α-Fe (Supporting Information, Figure S2) and decrease in magnetic properties (Figure S3). This result strongly indicates that the $O_3$ treatment to remove organic ligands is requisite for the formation of high-performance nanocomposite magnets. These two NPs were then used to form $L1_0$-FePd/α-Fe NCMs (FePd/Fe NCMs) with hard/soft volume fractions of 44/56, 82/18, and 100/0. XRD patterns (Figure 3a) of the $L1_0$-FePd/α-Fe (44/56) NCMs obtained in various annealing conditions indicated that nanoscale $L1_0$-FePd and α-Fe phases were formed successfully. Temperature dependency of grain sizes of the hard and soft phases (Figure 3b) was calculated from half band widths of the XRD main peaks, that is, the $L1_0$-FePd(111) and α-Fe(110) peaks, utilizing the Scherrer equation. Each phase coalesced and grew to approximately 30 nm in size when annealed at 723 K. Growth of the α-Fe phase was suppressed to approximately 30 nm at annealing temperatures < 748 K, while its grain size was >30 nm when the annealing temperature exceeded 773 K. Moreover, a disordered face-centered cubic (fcc) FePd phase[21,22] was observed when the annealing temperature reached 823 K (Figure 3a). Therefore, 823 K was determined as the upper limit of the annealing temperature to obtain nanocomposite structure.

A microstructural analysis of the resulting FePd/Fe NCMs was conducted by TEM. Figure 4a−f shows the high-resolution TEM (HRTEM), fast Fourier transform (FFT) spots, and inverse FFT (IFFT) images of FePd/Fe (44/56) NCMs obtained by annealing at 723K. FFT spots also revealed that the annealed NPs consisted of $L1_0$-FePd and α-Fe. Referring to key diagrams of body-centered

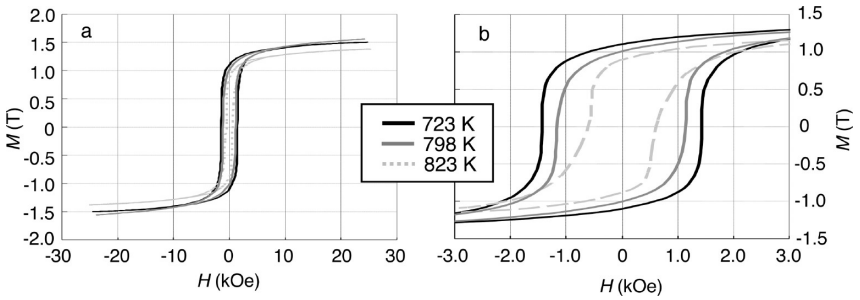


**Figure 5. (a) $M-H$ loops and (b) demagnetization curves of FePd/Fe (44/56) NCMs formed by annealing at various temperatures.**

cubic (bcc) ⟨111⟩ and fcc ⟨110⟩ zone axes (Supporting Information, Figure S4), the spots in Figure 4c,e were attributed to α-Fe(110)⟨111⟩ and $L1_0$-FePd(111)⟨110⟩, respectively. The interface between $L1_0$-FePd and α-Fe had an orientation relationship of α-Fe(110)//$L1_0$-FePd-(111) and α-Fe ⟨111⟩//$L1_0$-FePd ⟨110⟩, indicating that the close packed planes of both phases contacted coherently at the interface with slight distortion. The α-Fe(110) lattice plane gradually expanded from 0.203 to 0.205 nm, while the $L1_0$-FePd(111) lattice plane gradually shrank from 0.219 to 0.215 nm. The lattice mismatch between the two phases was 4.7%, which was determined by dividing the difference of the lattice spacings between $L1_0$-FePd(111) and α-Fe(110) (0.215 − 0.205 = 0.010 nm) by the FePd(111) value (0.215 nm). The data in Figure 4 illustrate only selected cases of heteroepitaxial junctions, whereas our system is very likely to be characterized by an incredibly broad distribution of coincidence lattice relationships holding among the randomly interfaced $L1_0$-FePd and α-Fe nanometer-sized domains. At higher annealing temperatures, both phases became coarser rapidly, leading to noncoherent contact at the interface (Figure 4g−l). Additionally, because of the extreme phase-segregation, the soft phase size increased relative to the evaluated exchange length, which is approximately 10 nm in the case of Fe as a soft phase.[23] EDX line analysis of the annealed sample indicated that the $L1_0$-FePd and α-Fe phases had nanometer size distributions and that the $L1_0$-FePd and α-Fe phases were neighboring each other (Supporting Information, Figure S5). Consequently, it was clarified that the soft phase was in coherent contact with the hard phase within an exchange interaction length.

**Magnetic Properties.** We then investigated the dependency of the magnetic properties of the FePd/Fe NCMs on the annealing temperature and the hard/soft phase volume fraction. Magnetization curves of the FePd/Fe (44/56) NCMs formed by annealing at 723, 798, and 823 K (Figure 5) were obtained using a vibrating sample magnetometer (VSM) at room temperature. The magnetization process observed for the samples annealed below 798 K was characteristic of a single-phase hard magnet, which implies that these FePd/Fe NCMs behave magnetically like single magnets because of the effective exchange interaction. In contrast, the sample annealed at 823 K had a $M-H$ loop of two superimposed curves in the second quadrant, indicating that a section of the soft phase was no longer coupled with the hard phase because of enlargement of the soft phase or disorder of the $L1_0$-FePd phases. Thus, magnetization reversal of the α-Fe phase took place at low magnetic field, and that of the $L1_0$-FePd phase at relatively high magnetic field. The exchange coupling is discussed in detail later.

To clarify the ideal volume fraction of the hard/soft phases, the effect of the volume fraction of hard/soft phases (FePd/Fe = 44/56, 82/18, and 100/0) on the magnetic properties was investigated. The Pd/γ-$Fe_2O_3$ heterostructured NPs and pure Pd NPs were annealed at 723 and 773 K, and no large changes were observed in the size of $L1_0$-FePd phases among the three mixtures. XRD peaks for the $L1_0$-FePd hard phase were observed in the XRD patterns of all these FePd/Fe NCMs (Supporting Information, Figure S6), while the peak intensity of α-Fe(110) decreased with increasing Pd content. For the FePd/Fe (100/0) NCMs (molar ratio of Fe/Pd = 50/50) the diffraction peak of α-Fe(110) was absent, indicating only the $L1_0$-FePd hard phase formed. The crystalline sizes of both phases were evaluated with the Scherrer equation for the $L1_0$-FePd-(111) and α-Fe(110) peaks and were found to increase at higher annealing temperatures (Supporting Information, Figure S7). The size of the α-Fe phase was largely increased at annealing temperatures >748 K for the FePd/Fe (44/56) NCMs, while substantial coalescence was not observed for the FePd/Fe (82/18) NCMs annealed below 773 K.

Figure 6 presents the magnetization curves of the FePd/Fe NCMs with various hard/soft phase volume fractions formed by annealing at 723 and 773 K. The remanence clearly increased with increasing soft phase volume fraction at both annealing temperatures. In comparison, increases in the hard phase volume fraction resulted in increased coercivity, as observed in previous studies of the NdFeB and PrFeB systems.[1,4,5] The dependencies of saturation magnetization ($M_s$), remanent magnetization ($M_r$), $M_r/M_s$ ratio, coercivity ($H_c$), and maximum energy product ($(BH)_{max}$)

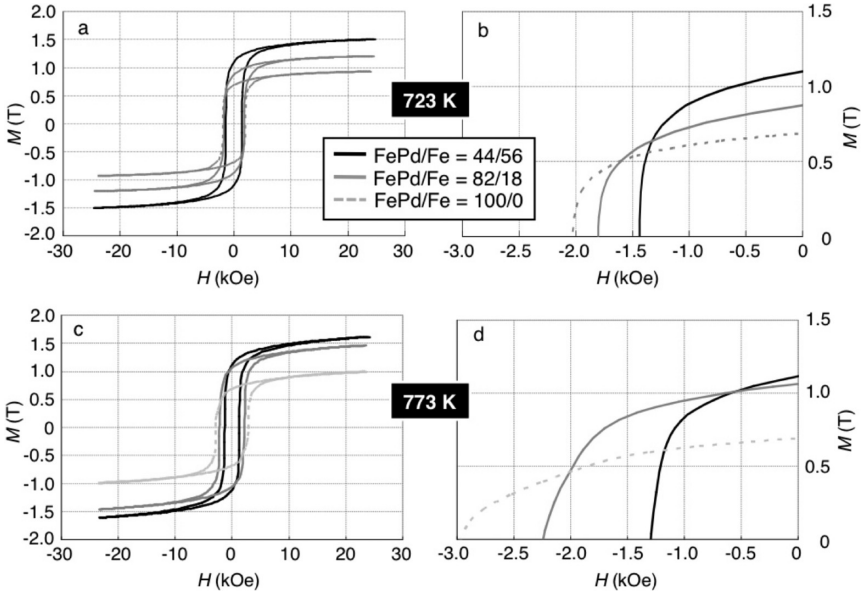


**Figure 6. (a,c) $M-H$ loops and (b,d) demagnetization curves at the second quadrant of FePd/Fe NCMs with various hard/soft phase volume fractions formed by annealing at (a,b) 723 and (c,d) 773 K.**

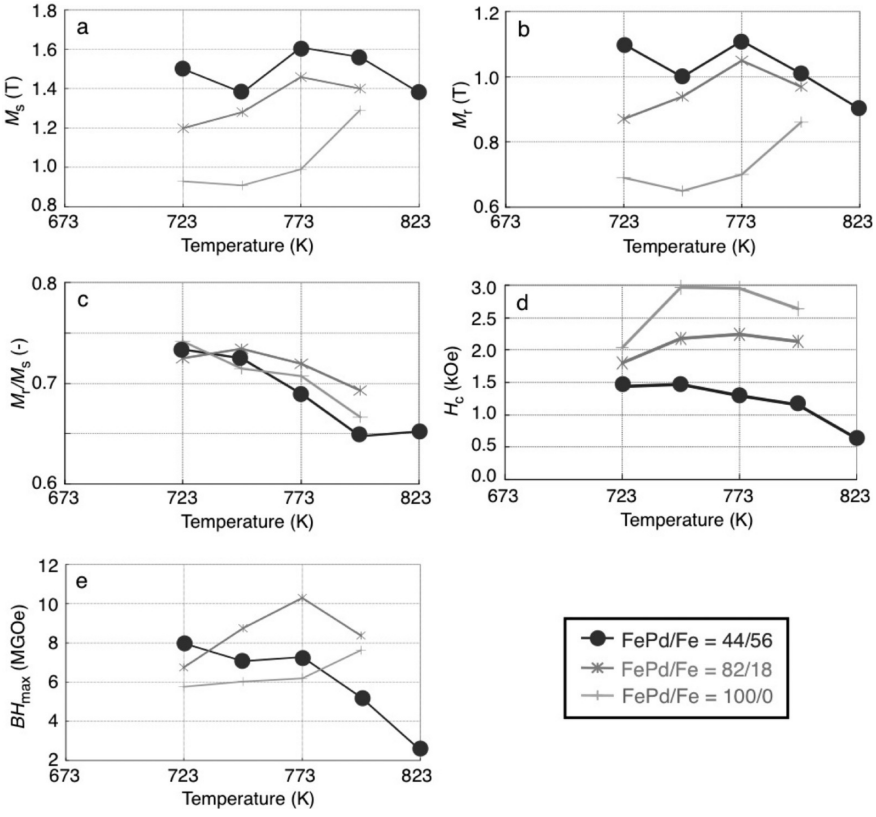


**Figure 7. Annealing temperature dependency of magnetic properties of the FePd/Fe NCMs with various hard/soft phase volume fractions: (a) saturation magnetization, $M_s$, (b) remanent magnetization, $M_r$, (c) $M_r/M_s$ ratio, (d) coercivity, $H_c$, and (e) maximum energy product, $BH_{max}$.**

on the annealing temperature are summarized in Figure 7. Both $M_s$ and $M_r$ were maximized at the annealing temperature of 773 K, and above this temperature they decreased because of coalescence of α-Fe and disorder of the $L1_0$-FePd phase. For the FePd single phase sample (FePd/Fe = 100/0), both $M_s$ and $M_r$ increased with the annealing temperature, probably because of the improvement of long-range order. In all samples, $M_r/M_s$ values decreased above 773 K, which can be explained by coalescence of the α-Fe phase and

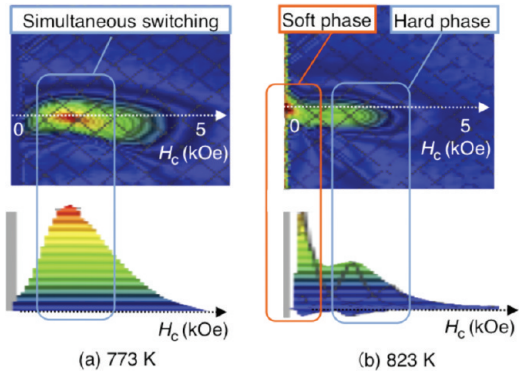


**Figure 8. FORC diagrams of the FePd/Fe (44/56) NCMs formed by annealing at (a) 773 and (b) 823 K.**

the resulting increase in the decoupled section of the soft phase at higher annealing temperatures. The decrease in $M_r/M_s$ for the FePd single phase might arise from the decoupling of $L1_0$ intragrain coupling by disordering of the $L1_0$ phase around the grain boundaries.

In consideration of $H_c$, the optimum annealing temperature was found to lie between 748 and 773 K. Rather than the disorder of the $L1_0$-FePd phase, a decrease in $H_c$ above 773 K was probably caused by the extreme phase-segregation of the $L1_0$-FePd and α-Fe phases and/or the coalescence of α-Fe, which resulted in an increase in the decoupled region with low $H_c$ (Supporting Information, Figure S8). The crystallographic anisotropy field, $H_a$, is described by the following well-known equation.[24]

$$H_a = 2K_u/M_s \quad (1)$$

where $K_u$ is magnetic anisotropy energy. For the $L1_0$-FePd phase, $K_u = 1.8$ MJ/m$^3$ and $M_s = 1.39$ T[25,26] give $H_a = 2.6$ T. Therefore, the maximum $H_c$ value for the FePd single phase without magnetic insulation is estimated at approximately 12% of the $H_a$ value or 3.0 kOe, which is comparable with other magnet systems.[27−30]

It is well-known that the highest $BH_{max}$ is obtained when the balance between the $M_r$ and $H_c$ values is optimum for good squareness in the $M-H$ loop. The $BH_{max}$ values are shown as a function of annealing temperature in Figure 7e. It is obvious that the $BH_{max}$ values of the NCMs are larger than that of the FePd single phase, demonstrating that formation of NCMs consisting of hard/soft phases increases $BH_{max}$ even though there is a trade-off between $M_r$ and $H_c$. In contrast to the FePd/Fe (82/18) NCMs, the $BH_{max}$ of the FePd (44/56) NCMs largely decreased with increasing annealing temperature along with $H_c$, because of a decrease in the average magnetic anisotropy with increasing soft phase volume fraction. These results strongly indicate that the averaging of magnetic anisotropy in NCMs needs to be considered when trying to increase $BH_{max}$. The FePd/Fe (82/18) NCMs formed by annealing at 773 K had the largest $BH_{max}$ of 10.3 MGOe among our samples, which is the largest value achieved to date for NCMs without using platinum or rare-earth elements.

**Analysis of Exchange Interaction with FORC Diagram.** Analysis of exchange interactions with a Henkel-plot or δM plot[31] requires care with limitations of the δM-plot that arise because of two assumptions: (1) all the magnetic NPs switch in a coherent rotation and (2) no domain walls exist even in the thermally demagnetized state.[32] We found from the δM-plot of NdFeB sinter magnet that the positive shift indicated the domain wall motion as shown in Supporting Information, Figure S9. A positive shift was also observed for thermally demagnetized nanocrystalline NdFeB magnet, even though this magnet has a grain size below a single domain size and intergrain exchange is decoupled. Therefore, the existence of domain walls inside grains in the thermally demagnetized state should be taken into account even if the grains are smaller than the single domain size, as pointed out by Stancu *et al*.[20] Thus, the δM-plot is not suitable for exchange interaction analysis without considering the origin of the demagnetized state. To overcome this limitation, we used a FORC diagram[33−36] for visualization of the exchange interaction of the FePd system. This method, which defines the ground state as a saturated state, allows us to interpret every magnetic event. As a result, we can ignore the existence of metastable domain walls, which lead to misinterpretation of the exchange coupling. There are some attempts to analyze nanocomposite multilayer systems with a FORC diagram. For example, Devies *et al*. applied FORC diagram analysis to the nanocomposite multilayer films, SmCo/Fe and FePt/FeNi systems, to separate reversible and irreversible processes of magnetic reversal.[37] They successfully separated reversible and irreversible processes with a FORC diagram and observed that the reversal process predominantly attributed to the Fe layer and the irreversible process was triggered by the reversal of SmCo phase. This means that they observed a part of exchange coupling phenomenon but did not focus on distinguishing the exchange coupling effect of the multilayer films. Moreover, it should be noted that their FORC diagram indicates no magnetically coherent rotation, for example, domain wall motion, which makes it difficult to dicuss the exchange coupling phenomena with such film samples. On the contrary, our NCM samples consist of magnetic NPs small enough to prevent the magnetic domain wall from participating the magnetic reversal process.[36] From this point of view, we adopted a FORC diagram to analyze the exchange coupling effect in our samples.

As discussed earlier, the XRD results (Supporting Information, Figure S6) revealed the formation of soft and hard phases after annealing of the mixture

of Pd/$\gamma$-$Fe_2O_3$ heterostructured NPs and pure Pd NPs under a reducing atmosphere. If each magnetic phase behaves independently, two peaks attributed to the hard and soft phases should appear in the FORC diagram. If the exchange coupling takes place between the hard and soft phases, the two peaks should merge into one. On the basis of this assumption, we measured and plotted FORC data sets (Figure 8) for the FePd/Fe (44/56) NCMs formed by annealing at 773 and 823 K, in which the soft phase sizes were quite different, whereas the hard phase sizes were constant. Only one peak was observed for the FePd/Fe NCMs formed at 773 K (Figure 8a), indicating that a magnetization switching occurred at the same magnetic field even though the soft and hard phases coexist in this sample. Moreover, this peak distributes on an $H_c$ axis, meaning that all phases are magnetically switching immediately at the same magnetic field, as observed in single domain NPs, that is, a reversal mechanism expected for the nanocomposite system. The peak distribution observed in the FORC diagram might be derived from the size distribution of the resulting phases. In comparison, for the FePd/Fe NCMs formed at 823 K (Figure 8b), two coercivity distribution peaks were observed in low and relatively high coercivity regions. The peak at $H_c$ = 0 kOe is attributed to the α-Fe soft phases and the peak at $H_c$ = 1.5 kOe from the $L1_0$-FePd hard phases. Especially, the peak at $H_c$ = 1.5 kOe deviates slightly below the $H_c$ axis due to the magnetostatic interaction with the magnetically switched α-Fe soft phases.[38] The FFT structural analysis of the TEM image for the FePd/Fe NCMs formed at 773 K (Figure 4) revealed that annealing at 773 K led to formation of a coherent hard/soft interface without any intermediate phases, meaning that a soft phase with optimum size was formed in Figure 4. Coalescence of the soft phase was easily confirmed for the FePd/Fe NCMs formed at 823 K (Figure 3b). In consideration of these microstructural analyses, it is concluded that the FORC diagram can detect coupling and decoupling portions of the magnetic phase. Additionally, both the coherency of the interface and optimization of size balance between the hard and soft phases are very important to effectively induce exchange coupling for an enhancement of the magnetic properties.

## CONCLUSIONS

We investigated the structural conditions required for NCMs with FePd/Fe. Annealing a mixture of Pd/$\gamma$-$Fe_2O_3$ heterostructured NPs and pure Pd NPs successfully formed $L1_0$-FePd/α-Fe NCMs with various hard/soft volume fractions. The largest $BH_{max}$ of 10.3 MGOe was achieved for $L1_0$-FePd/α-Fe (82/18) formed by annealing at 773 K. This temperature gave both a coherent interface and optimized sizes of the hard and soft phases to effectively induce exchange coupling. This exchange coupling was visualized with FORC diagram analysis of the magnetic interaction between the hard/soft phases, which is a valuable tool to improve the magnetic properties of NCMs.

## EXPERIMENTAL SECTION

**Synthesis of Pd/$\gamma$-$Fe_2O_3$ Heterostructured NPs.** Monodisperse trioctylphosphine-protected Pd (TOP-Pd) NPs (4.9 ± 0.3 nm) were synthesized according to a previous report.[39] HRTEM and XRD analyses revealed that these Pd NPs were polycrystalline. Anisotropically phase-segregated Pd/$\gamma$-$Fe_2O_3$ heterostructured NPs were synthesized by Pd-seed mediated synthesis.[11] The TOP-Pd NPs (Pd = 0.17 mmol) were dissolved in 1-octanol (20 mL), to which $Fe(acac)_3$ (0.43 mmol), oleylamine (6.8 mmol), and oleic acid (6.8 mmol) were added. After the $N_2$-bubbled solution was stirred at 180 °C for 1 h, the heat source was removed to allow the black solution to cool to room temperature. The resulting NPs were purified with 1-hexane/ethanol (1/2, v/v). The Pd/$\gamma$-$Fe_2O_3$ heterostructured NPs can be synthesized by using not only phosphine-protected Pd NPs but also amine-protected Pd NPs as seeds.[40]

**Sample Preparation for FePd/Fe NCMs.** NCMs with different volume fractions of hard/soft phases were produced by mixing the Pd/$\gamma$-$Fe_2O_3$ NPs with the TOP-Pd NPs in n-hexane. The mixtures were sonicated, and samples with Fe/Pd molar ratios of 80/20, 66/34, and 50/50 were obtained. The mixed samples were treated with 3000 ppm $O_3$ at 200 °C for 2 h to remove surface organic agents like TOP and prevent carbonization on α-Fe. After $O_3$ treatment, the samples were annealed under an atmosphere of Ar + 4% $H_2$ for 10 h at several temperatures to both induce interfacial atom diffusion and generate ordered $L1_0$-FePd/α-Fe NCMs.

**Measurements and Analyses.** Chemical compositions of the mixed samples before and after annealing were confirmed by X-ray fluorescence spectroscopy (XRF, JEOL JSX-3202C), which indicated no large changes in Fe/Pd molar ratios were observed for all samples. The FePd/Fe volume fractions for the annealed samples were evaluated from the chemical compositions using density values of FePd (9.75 g/cm$^3$) and α-Fe (7.86 g/cm$^3$). The mixtures of Pd/$\gamma$-$Fe_2O_3$ and TOP-Pd NPs with Fe/Pd molar ratios of 80/20, 66/34, and 50/50 were converted into $L1_0$-FePd/α-Fe NCMs with FePd/Fe volume fractions of 44/56, 82/18, and 100/0, respectively. XRD measurements (Rigaku Rint-2000) were carried out with Cu Kα radiation ($\lambda$ = 1.542 Å) at 50 kV and 300 mA. TEM (FEI Tecnai G2 F-30) studies were carried out with an operating voltage of 300 kV. Magnetic properties were evaluated by VSM (7410, Lake Shore). The demagnetization factor of each sample was set between 0.15 and 0.2, which was confirmed by the sintered samples. For a FORC diagram, the measurement conditions were as follows: (1) to realize a magnetic saturation state, a magnetic field of 15 kOe was applied; (2) measurement pitch for $H_A$ and $H_B$ was 0.15 kOe, and 200 FORCs were measured to construct the diagram; and (3) the FORC diagram was evaluated using a smoothing factor of 2.[41] All the samples were handled in an inert atmosphere during all the measurements and analyses to prevent oxidation of the α-Fe phase.

*Acknowledgment.* This work was supported by a Grant-in-Aid for Exploratory Research (No. 22655040) (T.T.).

*Supporting Information Available:* Phase diagram of the FePd system; XRD patterns of FePd/Fe NCMs with and without $O_3$ treatment; magnetic properties of FePd/Fe (44/56) NCMs with and without $O_3$ treatment; HAADF image and EDX line

analysis of the FePd/Fe (44/56) NCMs formed by annealing at 723 K; XRD patterns of the FePd/Fe NCMs with various hard/soft volume fractions formed by annealing at 723 and 773 K; crystalline sizes of $L1_0$-FePd and α-Fe phases in FePd/Fe (FePd/Fe = 44/56, 82/18, and 100/0) NCMs after annealing at various temperatures; speculated structural transformation of FePd/Fe NCMs at the annealing temperature above 773 K; δM plot of NdFeB sinter magnet and nanocrystalline NdFeB magnet. This material is available free of charge *via* the Internet at http://pubs.acs.org.

## REFERENCES AND NOTES


1. Coehoorn, R.; de Mooij, D. B.; Duchateau, J. P. W. B.; Buschow, K. H. J. Novel Permanent Magnetic Materials Made by Rapid Quenching. *J. Phys. Colloques* **1988,** *49*, C8–669–670.
2. Skomski, R.; Coey, J. M. D. Giant Energy Product in Nanostructured Two-phase Magnets. *Phys. Rev. B* **1993,** *48*, 15812–15816.
3. Sort, J.; Suriñach, S.; Muñoz, J. S.; Baró, M. D.; Nogués, J.; Chouteau, G.; Skumryev, V.; Hadjipanayis, G. C. Improving the Energy Product of Hard Magnetic Materials. *Phys. Rev. B* **2002,** *65*, 174420–1–5.
4. Kneller, E. F.; Hawig, R. The Exchange Spring Magnet: A New Material Principle for Permanent Magnets. *IEEE Trans. Magn.* **1991,** *27*, 3588–3600.
5. Wu, Y. Q.; Ping, D. H.; Hono, K.; Hamano, M.; Inoue, A. Microstructural Characterization of an α-Fe/$Nd_2Fe_{14}B$ Nanocomposite Magnet with a Remaining Amorphous Phase. *J. Appl. Phys.* **2000,** *87*, 8658–8665.
6. Schrefl, T.; Fidler, J.; Kronmüller, H. Remanence and Coercivity in Isotropic Nanocrystalline Permanent Magnets. *Phys. Rev. B* **1994,** *49*, 6100–6110.
7. Li, S.; Gu, B.; Bi, H.; Tian, Z.; Xie, G.; Zhu, Y.; Du, Y. Role of Amorphous Grain Boundaries in Nanocomposite NdFeB Permanent Magnets. *J. Appl. Phys.* **2002,** *92*, 7514–7518.
8. Rui, X.; Shield, J. E.; Sun, Z.; Xu, Y.; Sellmyer, D. J. In-Cluster-Structured Exchange-Coupled Magnets with High Energy Densities. *Appl. Phys. Lett.* **2006,** *89*, 122509–1–3.
9. Zeng, H.; Li, J.; Liu, J. P.; Wang, Z. L.; Sun, S. Exchange-Coupled Nanocomposite Magnets by Nanoparticle Self-Assembly. *Nature* **2002,** *420*, 395–398.
10. Figuerola, A.; Fiore, A.; Corato, R. D.; Falqui, A.; Giannini, C.; Micotti, E.; Lascialfari, A.; Corti, M.; Cingolani, R.; Pellegrino, T.; *et al.* One-Pot Synthesis and Characterization of Size-Controlled Bimagnetic FePt-Iron Oxide Heterodimer Nanocrystals. *J. Am. Chem. Soc.* **2008,** *130*, 1477–1487.
11. Teranishi, T.; Wachi, A.; Kanehara, M.; Shoji, T.; Sakuma, N.; Nakaya, M. Conversion of Anisotropically Phase-Segregated Pd/γ-$Fe_2O_3$ Nanoparticles into Exchange-Coupled fct-FePd/α-Fe Nanocomposite Magnets. *J. Am. Chem. Soc.* **2008,** *130*, 4210–4211.
12. Teranishi, T.; Inoue, Y.; Nakaya, M.; Oumi, Y.; Sano, T. Nanoacorns: Anisotropically Phase-Segregated CoPd Sulfide Nanoparticles. *J. Am. Chem. Soc.* **2004,** *126*, 9915–9916.
13. Teranishi, T.; Saruyama, M.; Nakaya, M.; Kanehara, M. Anisotropically Phase-Segregated Pd–Co–Pd Sulfide Nanoparticles Formed by Fusing Two Co–Pd Sulfide Nanoparticles. *Angew. Chem., Int. Ed.* **2007,** *46*, 1713–1715.
14. Teranishi, T.; Saruyama, M.; Kanehara, M. CdPd Sulfide Heterostructured Nanoparticles with Metal Sulfide Seed-Dependent Morphologies. *Chem. Commun.* **2009,** 2724–2726.
15. Teranishi, T.; Saruyama, M.; Kanehara, M. Synthesis and Structure-Specific Functions of Patchy Nanoparticles. *Chem. Lett.* **2009,** *38*, 194–199.
16. Teranishi, T.; Saruyama, M.; Kanehara, M. Seed-Mediated Synthesis of Metal Sulfide Patchy Nanoparticles. *Nanoscale* **2009,** *1*, 225–228.
17. Gu, H.; Yang, Z.; Gao, J.; Chang, C. K.; Xu, B. Heterodimers of Nanoparticles: Formation at a Liquid–Liquid Interface and Particle-Specific Surface Modification by Functional Molecules. *J. Am. Chem. Soc.* **2005,** *127*, 34–35.
18. Mokari, T.; Sztrum, C. G.; Salant, A.; Rabani, E.; Banin, U. Formation of Asymmetric One-Sided Metal Tipped Semiconductor Nanocrystal Dots and Rods. *Nat. Mater.* **2005,** *4*, 855–863.
19. Casavola, M.; Buonsanti, R.; Caputo, G.; Cozzoli, P. D. Colloidal Strategies for Preparing Oxide-Based Hybrid Nanocrystals. *Eur. J. Inorg. Chem.* **2008,** 837–854.
20. Stancu, A.; Bissell, P. R.; Chantrell, R. W. Interparticle Interactions in Magnetic Recording Media as Obtained from High-Order Measurements by a Preisach Model. *J. Appl. Phys.* **2000,** *87*, 8645–8652.
21. Issro, C.; Abes, M.; Püschl, W.; Sepiol, B.; Pfeiler, W.; Rogl, P. F.; Schmeber, G.; Soffa, W. A.; Kozubski, R.; Pierron-Bohnes, V. Atomic Ordering and Magnetism in L10 Ordered FePd Alloys. *Metall. Mater. Trans. A* **2006,** *37A*, 3415–3422.
22. Issro, C.; Püschl, W.; Pfeiler, W.; Rogl, P. F.; Soffa, W. A.; Acosta, M.; Schmeber, G.; Kozubski, R.; Pierron-Bohnes, V. Temperature-Driven Changes of Order and Magnetism in FePd Thin Films and Thin Foil. *Scr. Mater.* **2005,** *53*, 447–452.
23. Kawamura, J.; Sato, K.; Hirotsu, Y. Fabrication of Exchange-Coupled α-Fe/$L1_0$-FePd Nanocomposite Isolated Particles. *J. Appl. Phys.* **2004,** *96*, 3906–3911.
24. For Example: Hilzinger, H. R.; Kronmüller, H. Analytical Derivation of Spin Configuration and Intrinsic Coercive Field of a Narrow Domain Wall. *Phys. Stat. Solid. (b)* **1973,** *59*, 71–77.
25. Goo, N. H. Formation of Hard Magnetic $L1_0$-FePt/FePd Monolayers from Elemental Multilayers. Ph.D. Thesis, University of Stuttgart, 2007.
26. Al Ghaferi, A. A. Deformation and Dislocations TEM Images Simulation of $L1_0$ FePd. Ph.D. Thesis, University of Pittsburgh, 2006.
27. Ahmad, I; Davies, H. A.; Buckley, R. A. The Effect of Nd Content on the Structure and Properties of Melt Spun Nd-Rich NdFeB Alloys. *J. Magn. Magn. Mater.* **1996,** *157/158*, 31–32.
28. Hirotsu, Y.; Sato, K. Growth and Atomic Ordering of Hard Magnetic $L1_0$-FePt, FePd and CoPt Nanoparticles Studied by Electron Microscopy: Alloy System and Particle Size Dependence. *J. Ceram. Proc. Res.* **2005,** *6*, 236–244.
29. Hou, Y.; Kondoh, H.; Kogure, T.; Ohta, T. Preparation and Characterization of Monodisperse FePd Nanoparticles. *Chem. Mater.* **2004,** *16*, 5149–5152.
30. Yu, C. C.; Yao, Y. D.; Chou, S. C. Magnetic Properties of FePd Films Grown on Si Antidots. *J. Magn. Magn. Mater.* **2007,** *310*, 2333–2335.
31. Cui, B. Z.; Han, K.; Garmestani, H.; Su, J. H.; Schneider-Muntau, H. J.; Liu, J. P. Enhancement of Exchange Coupling and Hard Magnetic Properties in Nanocomposites by Magnetic Annealing. *Acta Mater.* **2005,** *53*, 4155–4161.
32. Cui, B. Z.; O'Shea, M. J. Hard Magnetic Properties of Rapidly Annealed NdFeB/Co Films and Intergrain Interactions. *J. Magn. Magn. Mater.* **2004,** *279*, 27–35.
33. Pike, C. R.; Ross, C. A.; Scalettar, R. T.; Zimanyi, G. First-Order Reversal Curve Diagram Analysis of a Perpendicular Nickel Nanopillar Array. *Phys. Rev. B* **2005,** *71*, 134407-1–12.
34. Winklhofer, M.; Zimanyi, G. T. Extracting the Intrinsic Switching Field Distribution in Perpendicular Media: A Comparative Analysis. *J. Appl. Phys.* **2006,** *99*, 08E710-1–3.
35. Wehland, F.; Stancu, A.; Rochette, P.; Dekkers, M. J.; Appel, E. Experimental Evaluation of Magnetic Interaction in Pyrrhotite Bearing Samples. *Phys. Earth Planet. Inter.* **2005,** *153*, 181–190.
36. Dumas, R. K.; Liu, K.; Li, C.-P.; Roshchin, I. V.; Schuller, I. K. Temperature Induced Single Domain–Vortex State Transition in Sub-100 nm Fe Nanodots. *Appl. Phys. Lett.* **2007,** *91*, 202501-1–3.
37. Davies, J. E.; Hellwig, O.; Fullerton, E. E.; Jiang, J. S.; Bader, S. D.; Zimányi, G. T.; Liu, K. Anisotropy Dependence of Irreversible Switching in Fe/SmCo and FeNi/FePt Exchange Spring Magnet Films. *Appl. Phys. Lett.* **2005,** *86*, 262503-1–3.

38. Davies, J. E.; Hellwig, O.; Fullerton, E. E.; Denbeaux, G.; Kortright, J. B.; Liu, K. Magnetization Reversal of Co/Pt Multilayers: Microscopic Origin of High-Field Magnetic Irreversibility. *Phys. Rev. B* **2004,** *70*, 224434-1–8.
39. Kim, S.; Park, J.; Jang, Y.; Chung, Y.; Hwang, S.; Hyeon, T. Synthesis of Monodisperse Palladium Nanoparticles. *Nano Lett.* **2003,** *3*, 1289–1291.
40. Sato, R.; Kanehara, M.; Teranishi, T. Homoepitaxial Size Control and Large-Scale Synthesis of Highly Monodisperse Amine-Protected Palladium Nanoparticles. *Small* **2011,** *7*, 469–473.
41. Roberts, A. P.; Pike, C. R.; Verosub, K. L. First-order Reversal Curve Diagrams: A New Tool for Characterizing the Magnetic Properties of Natural Samples. *J. Geophys. Res.* **2000,** *105*, 28461–28475.